SCEC Project #20177: Time-series InSAR analysis using ARIA standardized InSAR products in support of the Community Geodetic Model

Final Report

Gareth Funning, Simran Sangha and David Bekaert

Abstract

The SCEC Community Geodetic Model project is an attempt to produce a consensus set of processed InSAR and GNSS data that can be used by the scientific community for the purposes of constraining seismic hazard and tectonic behavior. We contribute to this effort using InSAR data from the Sentinel-1 satellites, processed routinely using a cloud-based system, under the Caltech-JPL Advanced Rapid Imaging and Analysis (ARIA) Center for Natural Hazards project (https://aria.jpl.nasa.gov/). The full archive of standardized Geocoded UNWrapped (GUNW) interferograms from 9 Sentinel-1 tracks that cover the entire state of California, is used to produce surface deformation velocity maps at a statewide scale. We validate these maps against GNSS velocity data, test the effectiveness of weather model-based troposphere corrections, and show some examples of deformation features apparent in the data, including subsidence of the San Joaquin Valley and shallow creep on the central San Andreas fault.

Data and methodology

The state of California is covered by Sentinel-1 SAR data from 9 tracks (ascending and descending geometries; Figure 1) that span a period from late 2014 through to the present day. Sentinel-1 Geocoded UNWrapped (GUNW) interferograms, produced by the Caltech-JPL Advanced Rapid Imaging and Analysis (ARIA) Center for Natural Hazards project (https://aria.jpl.nasa.gov/) cover a period from the initial acquisitions to early 2020. GUNW interferograms, also known as 'Standard Displacement Products' (https://aria.jpl.nasa.gov/products/standard-displacement-products.html) are interferograms produced by the ARIA system, based upon the ISCE processing software (Rosen et al., 2011), to standard specifications (90 m resolution, unwrapped, supplied with interferometric correlation, SAR amplitude, line-of-sight and geocoding information). Our data set (Table 1) is composed of interferograms that Our goal with this project was to incorporate these products into work flows that can advance the SCEC Community Geodetic Model (CGM) project.

We performed a time-series analysis using the open source 'ARIA-tools' (Buzzanga et al., 2020) and 'MintPy' (Yunjun et al., 2019) packages to estimate average line-of-sight surface velocities from the ARIA GUNW interferograms, along with their corresponding uncertainties. ARIA-tools is a suite of tools that enables downloading, quality-checking, mosaicking, cropping and masking of GUNW products in preparation for time series analysis. MintPy is a powerful time series analysis package that can produce Small BASeline subset (SBAS) solutions for deformation time series and deformation velocities from interferograms from a variety of

packages. Combined, these two packages present a robust standard workflow for producing deformation products suitable for inclusion in the CGM.

Table 1: Overview of Sentinel-1 data used in this project. 'A' or 'D' refer to ascending or descending acquisition geometries, respectively.

Sentinel-1 track number	Observation start	Observation end	Number of Sentinel-1 acquisitions	Number of interferograms
42 D	5/12/2015	11/11/2019	100	278
115 D	6/10/2015	2/8/2020	102	210
144 D	6/12/2015	11/18/2019	107	296
173 D	12/28/2014	1/1/2020	114	346
35 A	5/24/2015	11/11/2019	100	204
71 D*	5/14/2015	6/22/2019	91	259
137 A	5/7/2015	11/18/2019	118	350
166 A	6/26/2015	2/6/2020	60	202
64 A*	3/27/2015	6/28/2019	81	189

*Acquisitions after June 2019 are excluded from these tracks to avoid contamination of velocity estimates by the 2019 Ridgecrest earthquake sequence.

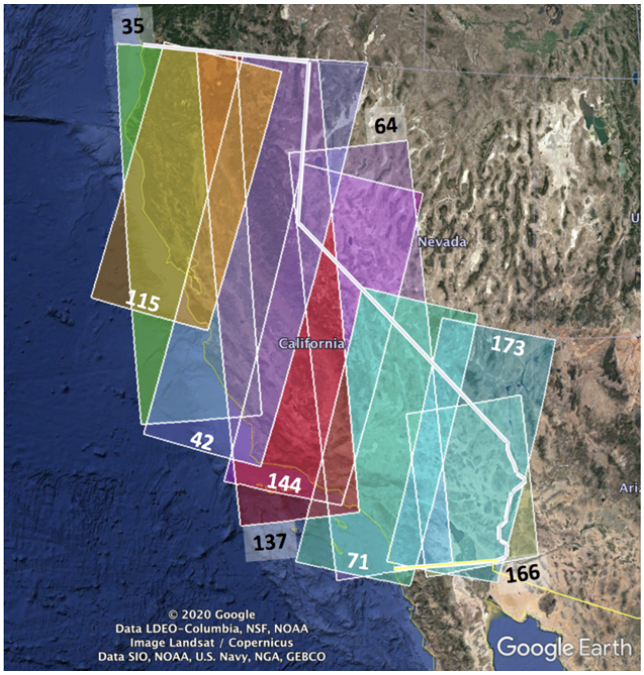

Figure 1: Overview of the Sentinel-1 ground track coverage of California. The entire state (white solid line) can be covered by a total of 9 Sentinel-1 tracks. Ascending (descending) track numbers are shown in white (black).

As tropospheric water vapor remains the principal source of noise in InSAR data, we test the efficacy of troposphere corrections from the GACOS project (Yu et al., 2018), based on the ECMWF HRES model, and evaluate velocities from both corrected and uncorrected data below.

Velocity results

We show results of our velocity analyses in Figure 2, with corresponding uncertainty estimates in Figure 3. Overall the features of the velocity estimates are consistent with expectations – the main pattern of velocities reverses in sign between ascending and descending tracks, consistent with a deformation field that is dominated by horizontal motions due to the San Andreas plate boundary fault system.

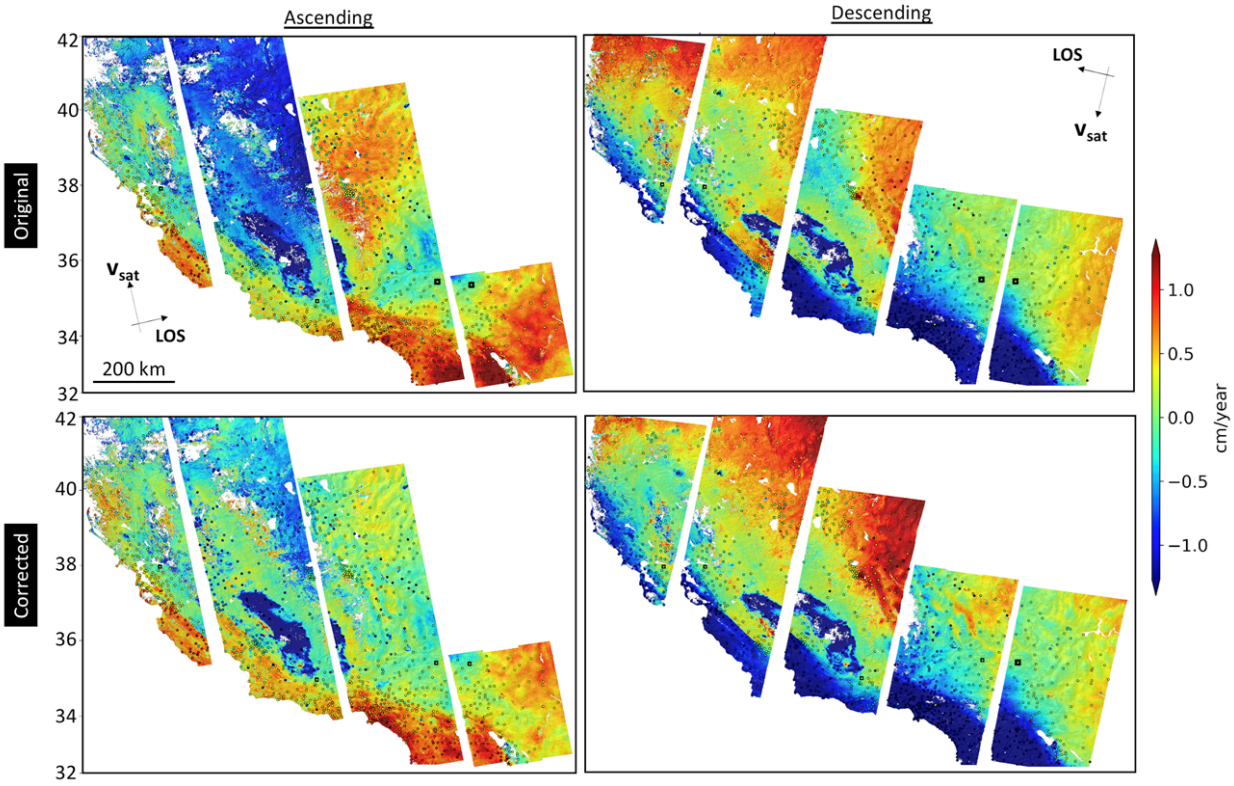

Figure 2: Line-of-sight surface velocities before (top row) and after (bottom row) applying tropospheric corrections. Left column shows velocities from ascending tracks; right column shows velocities from descending tracks. Velocities are referenced to a single GNSS station (black square) for each track; GNSS stations used for velocity comparisons are also marked (black dots) Note that as the Sentinel-1 tracks overlap at these latitudes by about a quarter to the east and west (see Figure 1) the different tracks are shown here in an 'exploded view' with the overlapping sections separated. Positive motions indicate motion of the ground towards the satellite, and vice-versa; thus the large negative velocity feature seen in the central tracks, corresponding to the San Joaquin Valley, is consistent with rapid subsidence – most likely due to groundwater extraction.

In addition, there are features common to both data sets (and with the same sign in both data sets) that indicate vertical motions. The most striking of these motions is the large negative deformation signal in the San Joaquin Valley, seen in all of the ascending and descending tracks that cover that region – this is consistent with rapid subsidence.

By visual inspection, we can see that the applied tropospheric corrections have some effect on the estimated velocities. Qualitatively, the corrected velocities look to have a 'flatter' overall appearance, which is particularly noticeable in the north and eastern portions of each track, away from the San Andreas system. This is particularly apparent in the ascending track data, which are all acquired in the early evening (around 6.05 pm PST), a time of more elevated and variable tropospheric activity (compared with the descending track data, acquired around 6.15 am PST), suggesting that there may be a larger contribution of tropospheric noise to remove from those data. This can also be determined from the velocity uncertainties (Figure 3) which show the uncertainties for the ascending data were larger than those for the descending data when uncorrected, but at a similar level when corrected for troposphere noise.

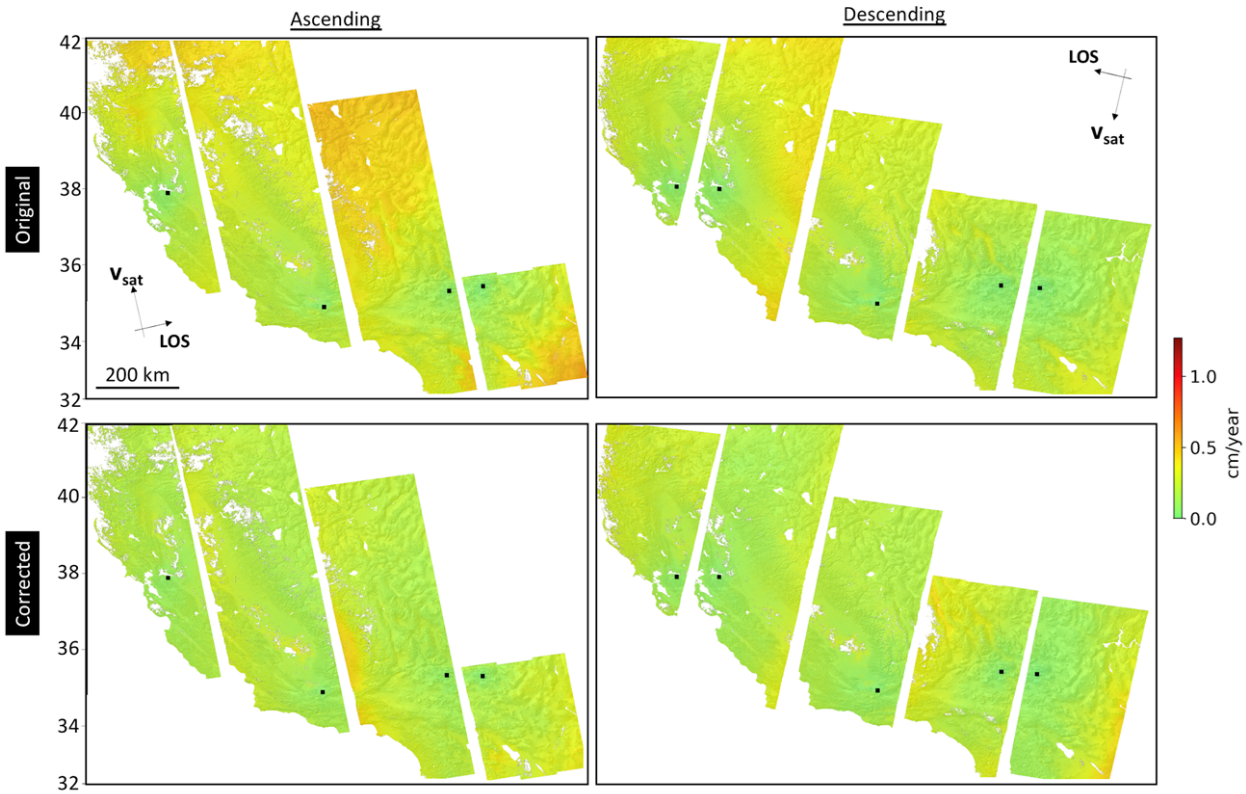

Figure 3: Uncertainties (1-sigma) for the velocities shown in Figure 2. Overall, we see a reduction in uncertainty for the corrected data (bottom row) compared with the original, uncorrected data (top row), suggesting that the GACOS troposphere correction used is effective at mitigating the effects of noise on our velocity results.

InSAR-GPS velocity comparison

Although estimating uncertainties can show the improved precision of velocity estimates afforded by troposphere corrections, they cannot show whether or not those velocity estimates are more accurate. For that, we must compare our velocities against independent data – from continuous GNSS stations. InSAR measures deformation velocities mapped into the line-of-sight (LOS) direction, and so to produce a comparable measure of velocity from GNSS data, we project GNSS velocities for the same interval from stations covered by each track estimated from the UNAVCO/NOTA (Network Of The Americas) solutions into the LOS of each track (Figure 4). In general we find that for 6 out of 9 tracks the root-mean-squared (RMS) difference between the InSAR and GNSS velocities reduces with the troposphere correction. After correction, we find an overall average RMS difference of 0.68 cm/yr.

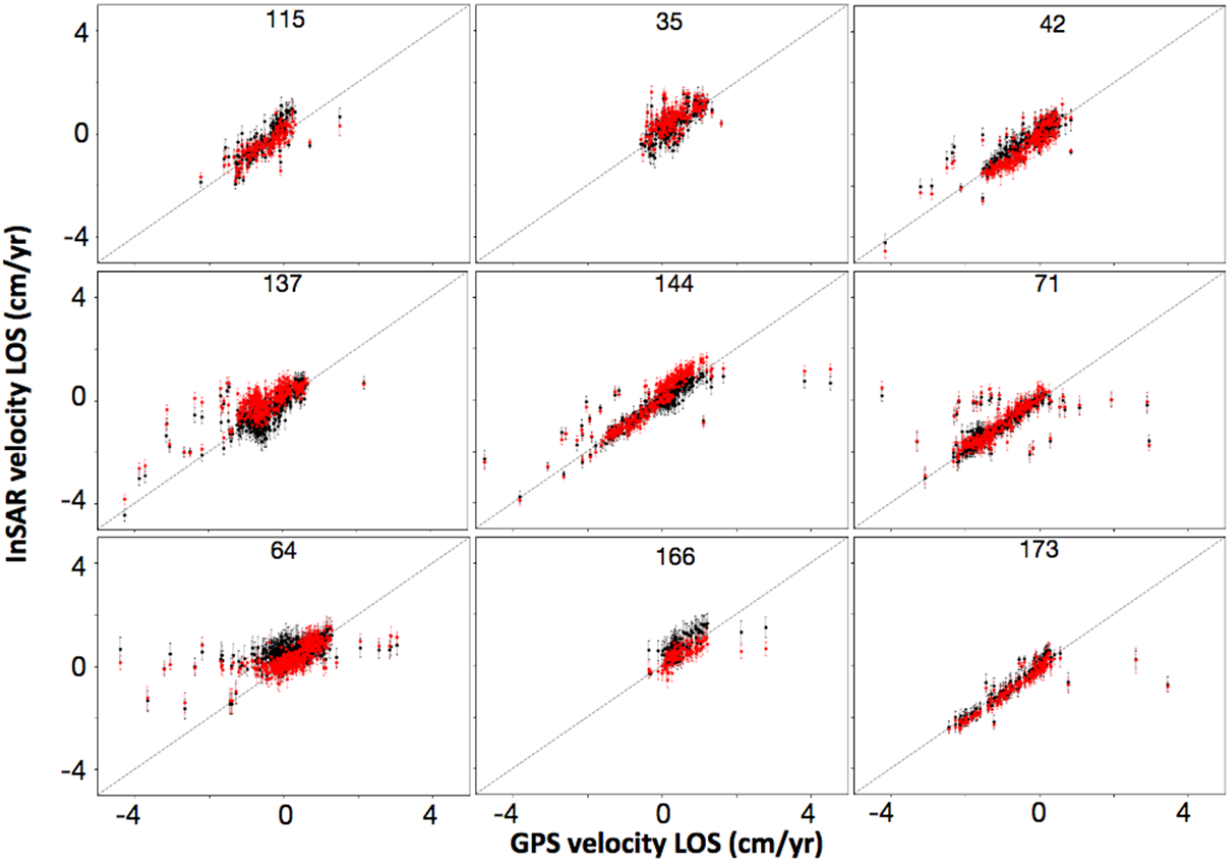

Figure 4: InSAR-GNSS comparison scatter plots of collocated line-of-sight rates before (black) and after (red) GACOS corrections. Error-bars correspond to 1-sigma. Black 1:1 lines are shown for comparison; in general, we find closer agreement between GNSS and the corrected InSAR velocities. Rates outside of the ± 5 cm/yr range have been excluded here; we suspect that disagreements at these larger deformation rates are due to aliasing of the InSAR signal.

Case study: Central San Andreas creep

To demonstrate the possibilities for geophysical analysis using these InSAR velocity maps, we show some preliminary results of surface creep rate analysis. Using the method of Jin and Funning (2017), we take regularly-spaced, strike-perpendicular profiles along the fault (2 km spacing, 4 km half-length, sampling data within 1 km on either side of the profile line), and fit pairs of straight lines with a common gradient to the data on either side of the fault (e.g. Figure 5). The surface velocity offsets we estimate in this way for each data set can be decomposed into two components of surface offset rate across the fault; we assume that all horizontal deformation is in the fault-parallel direction, which is generally valid in the absence of nontectonic deformation. In this way we are able to measure the southeastward decline in creep rates from a peak of ~25 mm/yr in the center of the creeping segment, down to zero at Cholame (Figure 6).

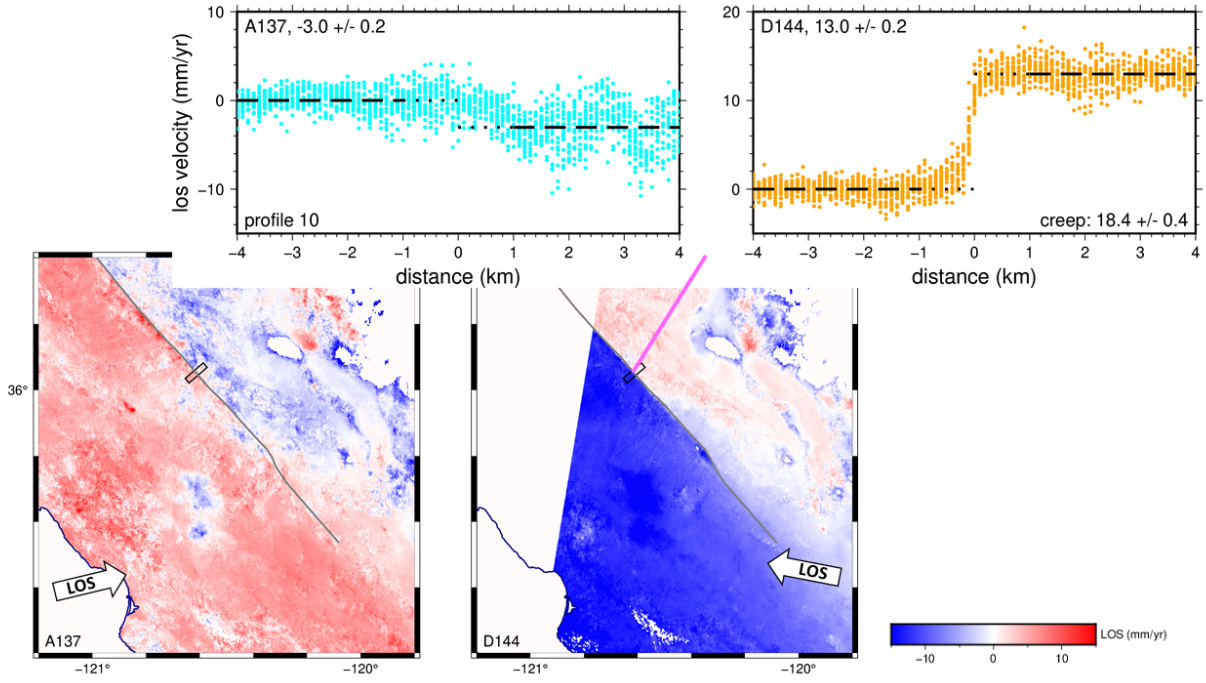

Figure 5: Deformation on the southern end of the central San Andreas fault 'creeping segment'. Lower panels: Map patterns of InSAR deformation velocities from ascending track 137 ('A137', lower left) and descending track 144 ('D144', lower right), showing sharp discontinuities in velocity, with opposite senses of offset, at the San Andreas fault (black line), consistent with surface creep on that structure. Black rectangle shows location of the example profile. Upper panels: Profile offsets estimated for both datasets. Black dashed lines are best-fit lines fitted to data between 4 km and 1 km of the fault on either side, with a common gradient (data are detrended using these best-fit gradients); the difference in y-axis intercept is used as an estimate of the shallow fault offset for each data set, and used to estimate creep rate.

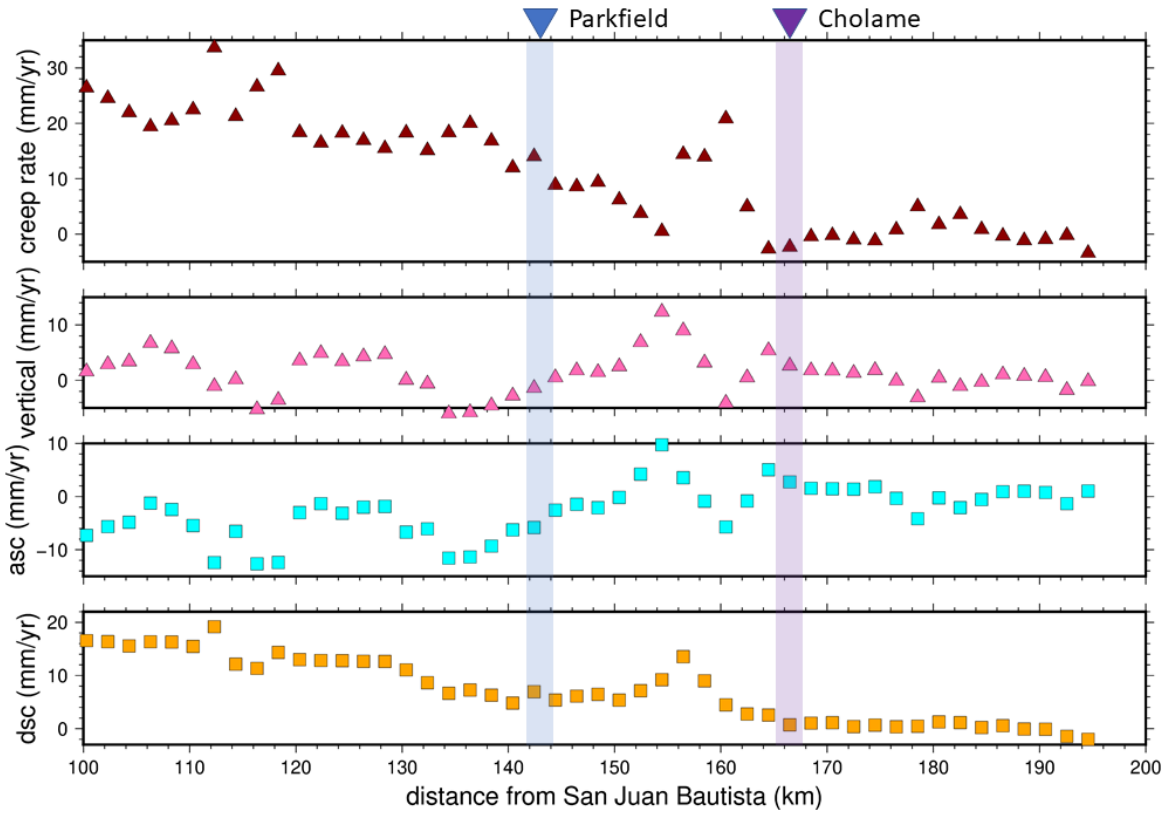

Figure 6: Summary of creep rate estimates along the southern creeping segment of the central San Andreas fault. Top panels: Estimates of fault-parallel ('creep rate') and vertical offset rates, estimated from decomposition of ascending and descending velocity profile offsets. Positive vertical velocity offsets represent east-side up motion. Bottom panels: Profile offset rates for ascending track 137 ('asc') and descending track 144 ('dsc') datasets. Distances are measured southeastwards from San Juan Bautista, the start of the creeping segment. Overall, the creep rate declines from 25 mm/yr in the center of the creeping segment to zero at Cholame (purple bar). We attribute deviations from this overall trend (at 110–120 km, and 155–165 km) to nontectonic deformation at those locations.

Summary and next steps

We have produced Sentinel-1 InSAR velocity maps covering the whole state of California using standard product interferograms from the ARIA project, using over 2000 interferograms from 9 tracks. Qualitatively and quantitatively, these velocity maps are improved with the inclusion of troposphere corrections from the GACOS project in the estimation process – the pattern of InSAR surface velocities appears flatter, and uncertainties are smaller in most cases (with a reduced RMS for 6 out of 9 tracks). Our statewide analysis using standardized products allows us to capture earthquake-cycle processes e.g. (fault creep) and subsidence. We are currently engaged in track-by-track comparisons of results with multiple other groups contributing to the CGM project, and hope to contribute time series in future CGM iterations.

References

Buzzanga, B., Bekaert, D. P. S., Hamlington, B. D., & Sangha, S. S. (2020) Toward sustained monitoring of subsidence at the coast using InSAR and GPS: An application in Hampton Roads, Virginia. Geophys. Res. Lett., 47, e2020GL090013. https://doi.org/10.1029/2020GL090013

Jin, L & G. J. Funning (2017) Testing the inference of creep on the northern Rodgers Creek fault, California, using ascending and descending persistent scatterer InSAR data, J. Geophys. Res. Solid Earth, 122, https://doi.org/10.1002/2016JB013535

Rosen, P.A., Gurrola, E.M., Sacco, G. & Zebker, H (2011) InSAR Scientific Computing Environment (ISCE) – the home stretch, Abstract IN42A-02 presented at 2011 Fall Meeting. AGU, San Francisco, CA. p. 5.

Yunjun, Z., H. Fattahi & F. Amelung (2019), Small baseline InSAR time series analysis: Unwrapping error correction and noise reduction, Computers & Geosciences, 133, 104331, https://doi.org/10.1016/j.cageo.2019.104331

Yu, C., Li, Z., Penna, N. T., & Crippa, P. (2018). Generic atmospheric correction model for interferometric synthetic aperture radar observations. J. Geophys. Res.: Solid Earth, 123, 9202– 9222. https://doi.org/10.1029/2017JB015305